Nano Research 2015, 8(9): 2810–2821
DOI 10.1007/s12274-015-0786-y
Research Article
ISSN 1998-0124
CN 11-5974/O4

Development of hydrophilicity gradient ultracentrifugation method for photoluminescence investigation of separated non-sedimental carbon dots

Li Deng, Xiaolei Wang, Yun Kuang, Cheng Wang, Liang Luo (✉), Fang Wang, and Xiaoming Sun (✉)

State Key Laboratory of Chemical Resource Engineering, Box 98, Beijing University of Chemical Technology, Beijing 100029, China

Received: 24 February 2015
Revised: 29 March 2015
Accepted: 5 April 2015

KEYWORDS
nanoseparation,
carbon dots,
hydrophilicity gradient,
pre-aggregation,
de-clustering,
photoluminescence mechanism

ABSTRACT

Carbon nanodots (CDs) formed by hydrothermal dehydration occur as mixtures of differently sized nanoparticles with different degrees of carbonization. Common ultracentrifugation has failed in sorting them, owing to their extremely high colloidal stability. Here, we introduce an ultracentrifugation method using a hydrophilicity gradient to sort such non-sedimental CDs. CDs, synthesized from citric acid and ethylenediamine, were pre-treated by acetone to form clusters. Such clusters "de-clustered" as they were forced to sediment through media comprising gradients of ethanol and water with varied volume ratios. Primary CDs with varied sizes and degrees of carbonization detached from the clusters to become well dispersed in the corresponding gradient layers. Their settling level was highly dependent on the varied hydrophilicity and solubility of the environmental media. Thus, the proposed hydrophilicity-triggered sorting strategy could be used for other nanoparticles with extremely high colloidal stability, which further widens the range of sortable nanoparticles. Furthermore, according to careful analysis of the changes in size, composition, quantum yield, and transient fluorescence of typical CDs in the post-separation fractions, it was concluded that the photoluminescence of the as-prepared hydrothermal carbonized CDs mainly arose from the particles' surface molecular state rather than their sizes.

1 Introduction

After their accidental discovery during the electrophoretic purification of single-wall carbon nanotubes (SWCNTs) [1], carbon nanodots (CDs) have gained research relevance as novel carbon nanomaterials [2–4]. CDs have been found to be composed of sp^2-bonded carbon, similar to nanocrystalline graphite [2]. Compared with bulk graphite, owing to their sub-10-nm size, CDs exhibit strong quantum effects, and consequently display fascinating and unique optical properties. Their high photoluminescence

Address correspondence to Liang Luo, luoliang@mail.buct.edu.cn; Xiaoming Sun, sunxm@mail.buct.edu.cn

(PL) quantum yield (QY), high photostability, anti-photobleaching, low toxicity, good biocompatibility, and non-blinking make CDs an excellent alternative to semiconducting quantum dots (QDs), for applications such bioimaging, sensing, and optoelectronics [5–10].

In this regard, tremendous research efforts have been devoted to investigating CDs' PL mechanism and optimizing methods for their synthesis. The two main classes of methods, physical and chemical, have been proposed for low cost and large-scale production. Physical (or "top-down") methods include arc discharge, laser ablation, and plasma treatment [1, 11, 12]. Chemical (or "bottom-up") methods include combustion, thermal or hydrothermal oxidation, microwave or ultrasonic treatment, and confined synthesis [10, 13–15]. For practical bio-applications, the facile and economic manipulation of size, chemical composition, and surface properties is particularly important; thus, hydrothermal or microwave reactions are attractive choices, permitting design and control. In these reactions, molecules or polymers with multiple hydroxyl, carboxyl, and amine groups, such as citric acid and amines, are used as starting materials. Recently, Yang et al. reported a facile hydrothermal carbonization method based on citric acid and ethylenediamine for the fabrication of fluorescent CDs with a QY reaching 80%. These thermal carbonized CDs showed strong blue PL. Considering the complex and diverse structural characteristics among CDs, the origins of the PL phenomenon are still under active debate. Mechanisms such as the quantum size effect [7], triplet carbenes at the CDs' zigzag edges [16, 17], radiative recombination of excitons [2, 18], and molecular states (as for organic dyes) have all been suggested. Definite experimental evidence for the PL mechanism involving the size effect still requires further investigation, especially in terms of the effective nano-separation of CDs.

In recent years, the density gradient ultracentrifuge rate separation (DGURS) method emerged as an efficient way of sorting nanoparticles of different sizes, compositions, and morphologies [19–21]. This strategy also provided new opportunities to isolate and capture intermediate reaction products to observe and gain understanding of chemical reactions, growth processes, or phase transitions [22–24]. However, when this method was extended to separate CDs, the CDs were found to be highly resistant to sedimentation. CD surfaces contain many carboxylic acid moieties; subsequently, strong hydrogen bonding occurs between CDs and water. This endowed the CDs with high water solubility, protecting them from separation by DGURS.

In this study, we designed a hydrophilicity gradient ultracentrifuge separation technique utilizing the differences in solubility or colloidal stability of CDs in different media to cause their separation. The CDs were synthesized from citric acid and ethylenediamine, and pre-treated using acetone to form clusters. Solutions of water in ethanol with different volume ratios were used as the separation-layer gradient, which could provide not only the density difference but also, and more importantly, the hydrophilicity difference to trap CDs with specific solubilities. During the subsequent separation process, the pre-aggregated CDs were separated in one tube into groups with different carbonization degrees and sizes, depending on the difference in hydrophilicity of the centrifugal fractions. The proposed technique offers an effective strategy to separate material species that interact strongly with solvents and thus prove difficult to sedimentate. This work also provides insight into the PL mechanism of CDs. In all centrifugal fractions, we analyzed changes in CD size, composition, QY, and transient PL. The analyses provided solid evidence that the PL of the as-prepared thermal carbonized CDs mainly arose from the radiative recombination of excitons related to the particles' surface chemical groups, rather than their size difference.

2 Experimental

2.1 Reagents

Citric acid and ethylenediamine were purchased from Sigma-Aldrich. Ethanol and acetone were purchased from the Beijing Chemical Reagents Company. All reagents were used without further purification; deionized (DI) water was used in all experiments.

2.2 Preparation of carbon nanodots

CDs were synthesized by a hydrothermal treatment of

citric acid and ethylenediamine [10]. First, 1.75 g citric acid and 560 μL ethylenediamine were dissolved into 16 mL DI water. The solution was then transferred to a 50 mL polytetrafluoroethylene (Teflon)-lined autoclave and heated at 200 ℃ for 5 h. After the reaction, the solutions were cooled to room temperature either by a water bath or naturally.

2.3 Multifunctional gradient preparation

The separation-layer step gradient medium was created from 20%, 30%, 40%, and 50% (by volume) solutions of water in ethanol. For instance, a 2:8 volume ratio of water to ethanol was used to make the 20% solution. The step gradient was created directly in polyallomer Beckman centrifuge tubes by adding layers of solution to the tube with decreasing water concentrations. To make a (20% + 30% + 40% + 50%) gradient, 0.8 mL of 50% H_2O in ethanol was first added to the centrifuge tube, then 0.8 mL 40% H_2O in ethanol was slowly layered above the 50% layer. Subsequent layers were made following the same procedure, resulting in a gradient of both hydrophilicity and density along the centrifuge tube.

2.4 Typical centrifugation of CDs

The prepared colloidal solution of CDs was pre-treated by first diluting it to double its original volume using DI water and then adding a 20-fold volume of acetone to the diluted solution. This formed a seriflux containing clusters of CDs. The seriflux was deposited slowly into a 0.8 mL layer above the density gradient. The tube containing both seriflux and density gradient was centrifuged at 50,000 rpm for 12 h. After centrifugation, one sample was pipetted gently from each of 20 fractions (fraction 1 through fraction 20, referred to henceforth as f1 through f20, respectively) for further characterization. Each sample contained 200 μL liquid. The precipitated material at the bottom of the centrifuge tube was re-suspended into DI water through ultrasonic processing, forming f21. To facilitate subsequent testing, all fraction solutions were evaporated to remove the organic solvent, and then re-dissolved into DI water. Only typical fractions were sampled for the investigation of their optical properties and structure, to study both the separation principle and the factors influencing CDs' PL intensity.

2.5 Characterization

The optical absorption of the CDs was measured by UV–vis spectroscopy (UV-2501PC, Shimadzu, working in the range 300–1,100 nm), and the PL emission spectra was measured at an excitation wavelength of 340 nm on a Hitachi F-7000 PL spectrometer. The sizes of the CDs were measured using high-resolution transmission electron microscopy (HRTEM; JEOL, JEM-2100, 200 kV). FTIR spectra were measured on a Nicolet 6700 FTIR spectrometer. X-ray photoelectron spectroscopy (XPS) measurements were performed using a Thermo Electron ESCALAB 250 instrument with Al Kα radiation. Raman spectra were recorded on the Lab RAM ARAMIS Raman system with a 633 nm argon ion laser as excitation. The fluorescence decay of the carbon dots was measured by a picosecond time-resolved fluorescence spectrometer, using a Ti:sapphire regenerative amplifier (Spitfire, Spectra Physics) to generate the excitation pulses. The excitation pulse energy was approximately 100 nJ/pulse at a pulse repetition rate of 1 kHz, focused onto a spot with a diameter of less than 0.5 mm. PL collected in a 90-degree geometry was dispersed by a polychromator (250is, Chromex) and collected with a photon-counting streak camera (C5680, Hamamatsu Photonics). The data detected by digital photography (C4742-95, Hamamatsu) were routinely transferred to a computer for analysis with High-Performance Digital Temporal Analyzer (HPDTA) software. The spectral resolution was 2 nm and the temporal resolution was 2–100 ps, depending on the setting of the delay time range.

3 Results and discussion

3.1 Properties of original CDs

The CDs were prepared by the hydrothermal treatment of a solution of citric acid and ethylenediamine at 200 ℃ [10]. The as-prepared product was a brownish solution after dilution, which exhibited strong blue PL emission under UV light (Fig. 1(a) inset). The absorption spectrum of the as-prepared CDs has a typical peak at 340 nm; when excited at 340 nm, a maximum emission peak at 440 nm is observed (Fig. 1(b)). According to HRTEM image (Fig. 1(a)), most particles are amorphous in structure without

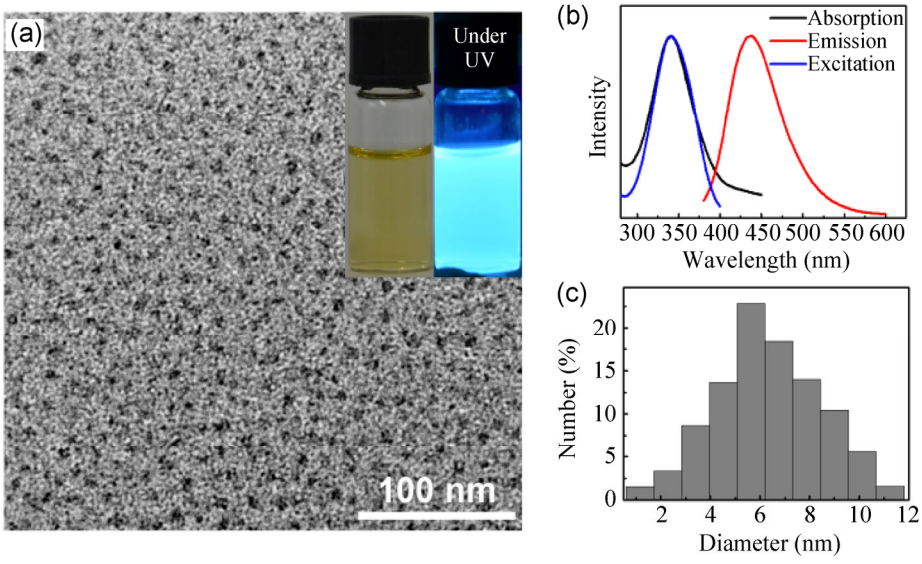

Figure 1 (a) HRTEM image of as-prepared CDs; inset: digital camera images under ambient light (left) and UV light (right). (b) UV–vis absorption (black), PL excitation (blue), and emission (red, excited at 340 nm) spectra of CDs. (c) Size distribution of CDs.

obvious lattices. A small amount of particles (<2%) show well-resolved lattice fringes with lattice spacings of 0.21, 0.26 and 0.33 nm, in accord with the (100), (020) and (002) facets, respectively, of graphitic carbon (Fig. S1 in the Electronic Supplementary Material (ESM)). The statistical diameter distribution data (Fig. 1(c)) shows a CD size range from 0.6 to 11.8 nm, indicating that the as-prepared CDs are not monodisperse owing to the inevitable heterogeneity of the hydrothermal reaction. Hence, the effective nanoseparation of the CDs is required to investigate their PL mechanism.

However, the as-prepared CDs were very stable in water, and, as mentioned previously, they resisted sedimenting out of water even with centrifuging at 90,000 rpm for 10 h (Fig. S2 in the ESM). A CsCl solution was also tried, with the intent of changing the dispersity of the CDs in water ("salt effect", Fig. S3 in the ESM), but the CDs still resisted effective separation after 36 h under 50,000 rpm centrifugation. This confirmed the CDs' good tolerance for physical salt concentrations in practical applications [10]. Hence, we changed solvent types to adjust the dispersity of CDs during the separation process. Alcohols were introduced as the common solvents, because of their good miscibility with water, as well as their weakened polarity, lowered hydroxyl ratio (corresponding to lower levels of hydrogen bonding), and lowered density compared to water. To test the efficacy of alcohols as solvents, equal amounts of diluted aqueous CD solutions were diluted using methanol, ethanol, isopropanol, and water as a control. After low-speed centrifugation at 12,000 rpm for 10 min, no precipitation occurred in water, while different amounts of brown precipitates were observed in the three alcohol-containing tubes, with the smallest and largest amounts in methanol and isopropanol, respectively (Fig. 2(a)). This verified that the difference in hydrophilicity, or ratio of hydroxyl molecules in the solvent, significantly affected the dispersity and sedimentation of CDs, which was key for their successful separation.

3.2 Separation of CDs using hydrophilicity gradient ultracentrifugation

In light of our observations concerning the hydrophilicity of the CDs' solvents, we designed a new separation method of hydrophilicity gradient ultracentrifugation to separate the CDs (Fig. 2(b)). For fine control over their separation, ethanol was chosen as the solvent to be mixed with water, due to its moderate hydroxyl ratio. A four-layer gradient medium with layers of varying density and hydrophilicity was made with 20%, 30%, 40%, and 50% DI/ethanol solutions, as explained in Section 2.3.

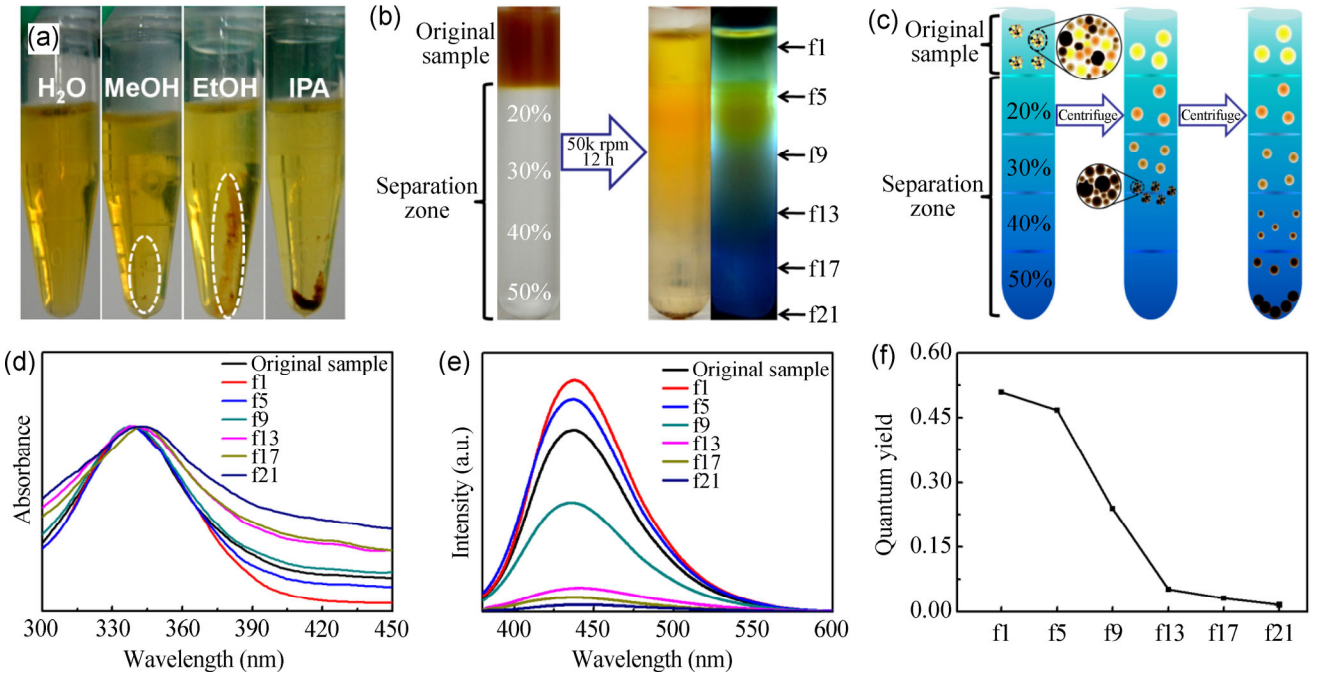

Figure 2 (a) Digital photographs of CD solutions after centrifugation in water, methanol (MeOH), ethanol (EtOH) and isopropanol (IPA). (b) Digital photographs of the centrifuge tube (under ambient light) before and (left: under ambient light, and right: under UV light) after centrifugation. (c) Scheme of proposed mechanism of separation: CDs were clustered at starting point and de-clustered at successive layers with increasing water content during sedimentation. (d) Normalized absorption and (e) PL spectra of original sample and separated fractions (excited at 340 nm; all samples diluted to the same absorbance). (f) QY variation of typical fractions, showing that more stable CDs have higher fluorescence.

In a stable gradient, the top layer containing CDs for separation would ideally have the lowest density of the layers in the gradient. Simultaneously, the layer needs a relatively high CDs concentration to meet the post-separation characterization requirements. We tried ethanol as the medium for the CD layer, but aggregation and precipitation were observed to occur at a high rate even without centrifugation, possibly due to the an excessively high concentration of CDs (Fig. S4 in the ESM; the solution in Fig. 2(a) is after a 50-fold dilution). When diluted with various volumes of acetone, stable suspensions were obtained even for highly concentrated aqueous solutions of CDs (Fig. S5 in the ESM), possibly due to the formation of "water-in-oil like" clusters of CDs in the water/acetone mixed solutions [25, 26]. This further increased the amount of target sample and provided a chance to improve the separation efficiency. The subsequent degree of detachment of fractions from the clusters was necessary for the separation effect. It was found to be closely related to the formation of the initial aggregates, which was indeed determined by the volume-ratio-induced size of the clusters. For the relatively highly concentrated clusters (20-fold acetone without the 2-fold water dilution), the QY measurements show obvious data jitter for the bottom fractions (Fig. S6 in the ESM). In much-diluted solutions of clusters (20-fold acetone, 100-fold water), we observe the fractions' passage through a very limited number of layers after centrifugation, implying incomplete separation (Fig. S7 in the ESM). Hence, during centrifugation, a dynamic balance occurred between sedimentation and detachment for the clusters, which prevented some fractions with high hydrophilicity from releasing with an excessively high concentration of clusters or causing incomplete separation of the CD solution with an excessively diluted concentration. After repeated testing, the optimized conditions for separation were determined. Two folds of water were added to each as-prepared CDs suspension, which were then diluted by 20 folds of acetone to form a homogeneous slurry. This was layered on top of the gradient medium.

The centrifugation was performed at 50,000 rpm for 12 h, as described in Section 2.4. After centrifugation, the CDs had become separated along the centrifuge tubes. With 365 nm UV irradiation, the PL intensity of the fractions in the centrifuge tube was observed to vary regularly from top to bottom. Figure 2(d) shows the UV–vis spectra of typical centrifugal fractions from the top to the bottom of centrifuge tube, as well as from the original unseparated sample. No obvious absorption-peak shift occurred in the separated fractions, except for a very limited shift of <10 nm for a few of the near-bottom fractions (such as f17). This indicates that the CDs across all fractions possessed essentially the same energy gap. The centrifuge tube in Fig. 2(b) shows an apparent color change, possibly due to the so-called inner filter effect [27]. Correspondingly, the PL spectra of the separated fractions (Fig. 2(e)) with excitation at 340 nm show no significant peak position difference, but the PL intensity of fractions monotonically decreases from the top to the bottom in the centrifuge tube, suggesting a decreasing QY of the fractions (Fig. 2(f)).

3.3 HRTEM analysis

The effectiveness of the hydrophilicity gradient separation technique and the differences in degree of carbonization are further confirmed by HRTEM (Fig. 3). Nine fractions, including f1, f5, f9, f11, f13, f15, f17, f19, and f21, were chosen as representative samples for HRTEM analysis. All are seen to be nearly monodisperse, with the exception of f1 and f5. These top fractions contain fish-scale-like polymer species with very weak contrast and blurry edges (Fig. S8 in the ESM), typical of polymer-like dehydrated species at the initial stages. Such species are very stable in the ethanol-rich environment, suggesting similarity in hydrophilicity between such species and their environments (Fig. 2(b)), and further confirms their polymer-like nature. The QYs of f1 and f5 both exceed 0.45, implying the high brightness of the polymer-like species under UV irradiation, which agrees with previous reports [28].

For middle fractions from f9 to f13, discrete, low-contrast nanoparticles with relatively clear edges are observed, implying increased condensing and carbonization degrees. They are 2–10 nm in size, much smaller than the CDs in the upper fractions (tens of nanometers in size). Interestingly, larger nanoparticles are located higher densities (size sequence: f9 > f11 > f13). This apparently abnormal phenomenon can be explained only by the fractions' different degrees of hydrophilicity. The larger CDs, on reaching a medium with hydrophilicity similar to their ambient medium, detach from their clusters and stabilize in that layer without visible sedimentation. In comparison, the smaller particles in f13–f21 have decreased hydrophilicity and are more compatible with the water-rich environment of the bottom half of the centrifuge tube.

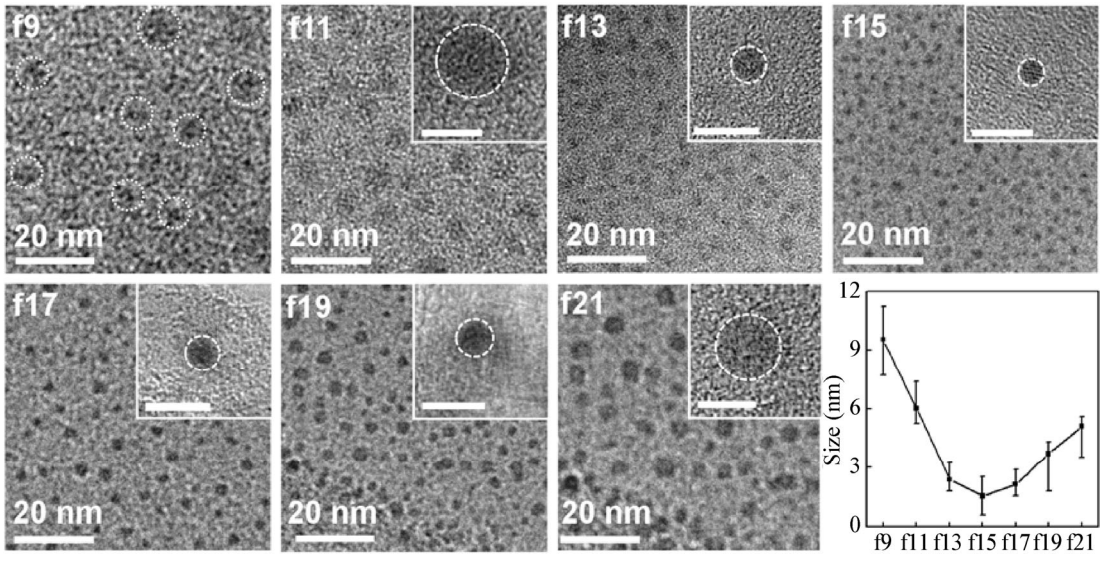

Figure 3 HRTEM images of typical fractions (from f9 to f21) and the statistics of CD size; inset: magnified HRTEM images of typical particles; scale bars are 5 nm.

The QYs of these fractions further demonstrates their differences in nature aside from their solubilities. The QY decreased dramatically from 0.48 to 0.05 in f9 and f13, respectively. We can infer that the abundance of polymer-like molecular states may be the origin of fluorescence in the CDs, since those in f9 are still polymer-like. The CDs in f13 are essentially more carbon-like.

For the bottom fractions from f15 to f21 shown in Fig. 3, the contrast increases and edges become clearer. The average CD size increases from 1.54 (f15) to 5.1 nm (f21). These CDs should be those which experienced the most complete carbonization during synthesis; their corresponding QYs remain lower than 0.05 (Fig. 2(f)). The sizes of 100–200 CDs per sample were measured (Fig. S9 in the ESM); the average particle size of each fraction is summarized in the bottom right graph of Fig. 3. In detail, the average size of fractions from top (f9) to bottom (f21) in the centrifuge tube gradually decrease from 9.5 (f9) to 1.54 nm (f15), and then increase again to 5.1 nm (f21). Interestingly, and differing from classic DGURS results, the fraction containing the smallest particles (f15) is located at the middle region of the centrifuge tube rather than the top region, because, as previously mentioned, the separation of these nanoparticles is based on the differences in hydrophilicity of the CDs. Species with different degrees of hydrophilicity naturally have various sizes. Specifically, according to the HRTEM results, the size distribution of CDs in the upper-half fractions exhibits a decreasing trend (Fig. 3). In the bottom-half fractions, the size distribution of CDs (from f15 to f21) exhibits an increasing trend (Fig. 3). Each separated fraction ceases sedimentation (Fig. 2(c)) after being discretized in a medium with certain hydrophilicity, even with elongated centrifugation times. Based on its movement features, the centrifuging method could be regarded as a modified isopycnic separation process. Importantly, the trend in fluorescence spectra and QYs indicated that the PL of CDs is not related to their size.

The carbonization degree is known to relate to the hydrothermal reaction time. Elongated hydrothermal treatment naturally strengthens the condensation and carbonization processes; therefore, we compared the PL spectra of the CDs in the above fractions (reacted for 5 h) with CDs prepared at varied hydrothermal treatment times of 7, 10, and 20 h. Interestingly, they showed very high similarities in their PL trend. Figure S10 in the ESM shows no peak shift, but the width of absorption peaks broadens and QY decreases with increased hydrothermal treatment time, which agrees with the trend of CDs in fractions in the centrifuge tube (Figs. 2(d) and 2(f)). We can infer that the hydrophilicity gradient separation redistributed the CDs according to their degree of carbonization (low at the top and high at the bottom of the tube, Fig. 2(c)). In addition, QY decreases with increasing degrees of carbonization, implying that the carbon content does not promote fluorescence in CDs.

3.4 FTIR analysis

For deeper insight into the chemical and structural differences of CDs in the different fractions, FTIR spectra are shown in Fig. 4. The vibrational intensity of the functional groups of CDs [10], such as stretching vibrations of C–OH at 3,430 cm^{-1} and C–H at 2,923 and 2,850 cm^{-1}, asymmetric stretching vibrations of C–NH–C at 1,126 cm^{-1}, bending vibrations of N–H at 1,570 cm^{-1}, and the vibrational absorption band of C=O at 1,635 cm^{-1}, decreases regularly as the fraction number (and density) increases from f1 to f17. This result suggests that the CDs in the fractions located near the top are richer in functional groups, while CDs with fewer functional groups sediment down to the bottom zone of the centrifuge tube. This trend

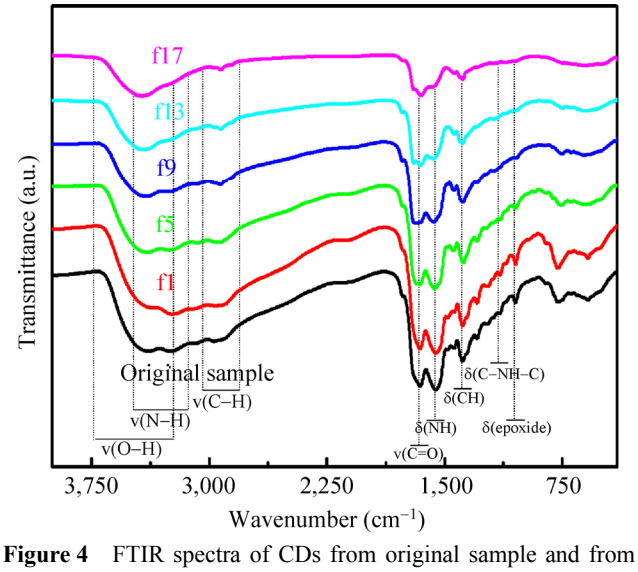

Figure 4 FTIR spectra of CDs from original sample and from typical fractions (f1, f5, f9, f13, and f17).

agrees with the HRTEM results showing the increase in degree of carbonization from f1 to f17.

3.5 X-ray photoelectron spectroscopy

XPS was used to investigate the surface states of CDs contained in the different fractions. The survey spectrum of the CDs before separation (Fig. 5(a)) shows three typical peaks attributed to C_{1s}, N_{1s}, and O_{1s}. Typical fractions after centrifugation were also tested to identify variations in their CDs' composition. The N/C ratio of CDs in different fractions (Fig. 5(b)) decreases as their f-number increases, indicating that relative N levels may influence the QY of CDs. Notably, the minimum N/C ratio reaches 0.16, which is still much higher than that of various N-doped CDs [29].

According to the HRTEM images, the very limited lattices we could find correspond to the (100), (020), and (002) facets of graphitic carbon (Fig. S1 in the ESM). We can infer that elemental N is not embedded into the main carbon structure, as it is in N-doped graphene quantum dots (N-GQDs). Related groups containing N in a molecular state would be released from the CDs as a result of carbonization processing, which may be the origin of the high QY for highly carbonized CDs. As shown in Fig. 5(c), the spectrum of C_{1s} in the typical CDs [30] can be deconvoluted into several single peaks corresponding to C=C/C=N (284.3 eV), C–C (284.9 eV), C–N (285.7 eV), C–O (286.5 eV), C=O (288.2 eV), and O–C=O (289.2 eV), consistent with the FTIR results. Three typical fractions (f1, f9, and f17) can provide a direct comparison. It is obvious that sp^2 graphitic C (284.3 eV) increases as the fraction number increases, while other functional groups such as C–N (285.7 eV), C–O (286.5 eV), C=O (288.2 eV), and COOH (289.2 eV) decrease. This confirms an increased carbonization degree and a corresponding decreased number of functional groups on the surface of the CDs, which also agrees with the HRTEM images (Fig. 3 and Fig. S8 in the ESM). According to the N_{1s} spectrum (Fig. 5(d)) [31], no apparent difference of N species exists for the three fractions, as C–N–C (399.5 eV), N–C_3 (400.6 eV), and N–H (401.5 eV) peaks appear in all three spectra. This further verifies that no change in the existence of N occurs; only the amount of N decreases (Fig. 5(b)). The FTIR and XPS results also demonstrate a trend in the amount of surface functional groups on CDs similar to that of the CDs' optical properties and hydrophilicity, the latter of which was the basis of the separation method (Fig. 2(c)).

3.6 Separation mechanism

Given the close relationship between carbonization

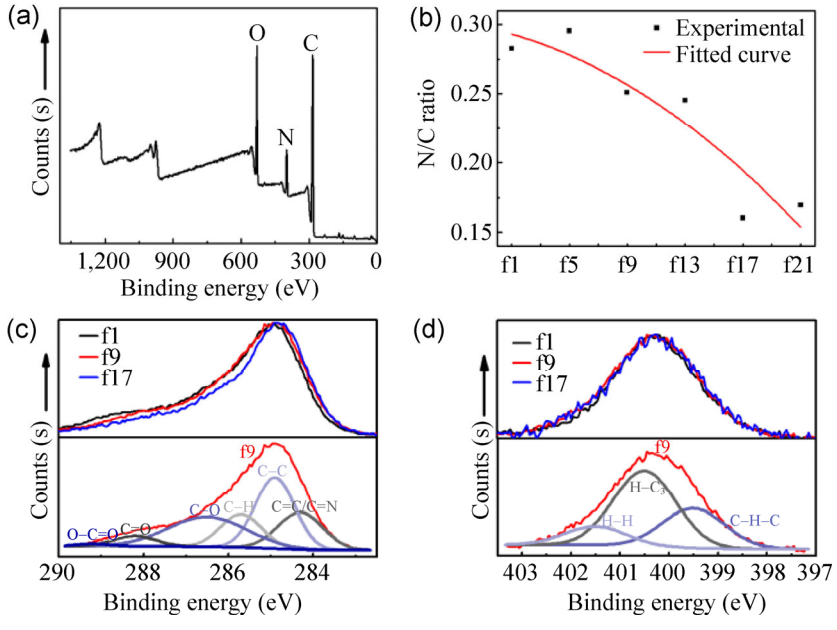

Figure 5 (a) Survey spectra of XPS measurements of CDs. (b) Experimental results and fitted curve of N/C ratio of CDs from separated fractions. (c) C_{1s} and (d) N_{1s} spectra of CDs from three typical fractions: f1, f9, and f17.

degree, morphology, and size based on the centrifugation results, the separation mechanism of CDs is expected to provide better understanding of the properties of CDs, especially their PL properties. Unlike the CDs obtained from physical synthesis methods, the CDs in this study were prepared by the hydrothermal treatment of a solution of citric acid and ethylenediamine, and contained abundant hydrophilic surface groups including –OH, –COOH, and $–NH_2$ which could form strong hydrogen bonds with solvents such as water. DI water/ethanol solutions were used as the gradient media for the separation zones, as mentioned previously, which provided both a density gradient relatively lower than that of pure water and a hydrophilicity gradient, intended to weaken the strong interactions between the surface-functionalized CDs and water. After treatment with acetone, the CDs formed tiny clusters (or possibly coiled polymeric structures), which were expected to promote the sedimentation of individual CDs as the target sample during the centrifugation. The surface groups present in CDs of each fraction were essentially the same, as all CDs were formed from the same chemical environment in one batch. However, the amount of surface groups present in each fraction differed, and this difference was dominant in the separation process. Specifically, the less-carbonized CDs had larger numbers of hydrophilic groups on their surface, and thereby would be more affected by the hydrophilicity of a medium. In this regard, when the clusters moved down the gradient medium, CDs with the strongest hydrophilicity (fish-scale-like polymer species) were the first to drift away from the clusters (de-cluster) and become dispersed in the top layer of the tube. As centrifugation progressed, the CD clusters moved to the next layer and conducted similar de-clustering behavior. For the bottom fractions (from f15 to f21), the CDs approached a molecular state similar to solid carbon particles with few surface groups. The corresponding separation process of these heavily carbonized particles was mainly determined by the sedimentation rate difference in the density gradient. Notably, no obvious Raman peaks typical of carbon vibrations occur (Fig. S11 in the ESM) even for highly carbonized CDs in the lower fractions (f17), indicating the poor crystallinity of the cores of the as-prepared CDs. Therefore, the results verified our assumption regarding the mechanism of the hydrophilicity gradient separation (Fig. 2(c)). As demonstrated in the aforementioned control experiments, aqueous CDs are almost non-sedimental owing to their abundant hydrophilic surface chemical groups. We approached this problem by pre-aggregating the individual CDs into clusters as the targets of separation, and effected this separation by inducing a subsequent irreversible dissociation. The form of the clusters permitted the sedimentation of individual CDs. The four layered ethanol/water solutions provided a gradient not only of the theoretically proper density, but also (and more importantly) of hydrophilicity for the separation. The pre-aggregated clusters underwent a sedimentation process directed by hydrophilicity-controlled de-clustering during the centrifugation; the separation effect depended strongly on the compatibility between the CDs' hydrophilicity and the mixed solvents' hydroxyl ratio. The CDs essentially ceased in sedimentation once they encountered their compatible media, even at elongated centrifugation times.

3.7 Transient fluorescence spectra

As a means to study the exciton delocalization, we measured the time-resolved PL decay (Fig. 6) for the original CDs and those in three typical separated fractions (f1, f9, and f17) at the emission peak (440 nm) with excitation at 340 nm. The decay curves are well fitted by two exponents, as listed in Table 1. An obvious change occurs (marked as red hollow circle) for the short-lifetime components of the CDs in the fractions from top to bottom of the centrifuge tube (f1–f17). The long-lifetime components can be attributed to the CDs' surface-state emission. In detail, the polymer-like CDs in f1 had the slowest PL decay of 5.15 and 14.86 ns. The mildly carbonized CDs in f9 followed with 4.60 and 12.91 ns. The most highly carbonized CDs in f17 had the fastest decays of 2.27 and 12.38 ns. However, the relatively obvious change in the short-lifetime components of the CDs in the three fractions was not as sharp as the size-dependent change in highly crystalline CdTe or CdSe QDs, which is attributed to the initially populated core-state recombination

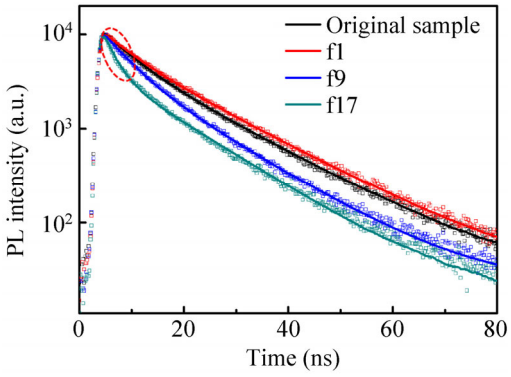

Figure 6 Transient PL spectra of CDs from the original sample and from three typical fractions: f1, f9, and f17.

Table 1 Fitting results of fluorescence lifetimes

	$\tau 1$ (ns)	$\alpha 1$	$\tau 2$ (ns)	$\alpha 2$	Total lifetime (ns)
Original sample	5.00	0.22	14.5	0.78	12.36
f1	5.15	0.17	14.86	0.83	13.25
f9	4.60	0.31	12.91	0.69	10.33
f17	2.27	0.29	12.38	0.71	9.41

[32, 33]. From the direct evidence of HRTEM results (Fig. 3 and Fig. S8 in the ESM), CDs in f1 possess the highest QY and polymer-like cluster structures, with no absolute structural "core". As the carbonization increased, namely, during the initial carbonization process, amorphous or poorly crystallized solid carbon cores formed, and the corresponding QY of the CDs in the middle fractions decreased dramatically from f5 to f13 (Fig. 2(f)) owing to the carbonization-induced decline of the original luminescent molecular-like cores and the sequential self-absorption of solid amorphous cores. For the CDs in the bottom fractions, the QY were relatively stable (Fig. 2(f)). Consequently, the PL decay measurement indicates that the emission of the as-prepared CDs depends more on their molecular states than their sizes. The changes in the short-lifetime components may be due to the self-absorption-induced quenching phenomenon as carbonization increases [34], which is a common and serious problem for fluorescent molecules in solid-state aggregates, including carbon-based materials. The limited change may have resulted from the limited degree of aggregation in the several-nanometers size range, which corresponds to the size distribution of the CDs. Compared with the PL decay of the original samples, the molecular state of most CDs in solution was that of polymer-like cross-linked clusters, such as those in f1–f5. These results confirmed Yang et al.'s hypothesis [28] of molecular state determining the optical properties, based on a series of investigations including CDs' pH-dependent behavior, solvent-dependent behavior, ferric ion-induced dynamic quenching, and high-power UV irradiation-induced destruction of PL centers.

3.8 Proposed PL mechanism of the CDs

The above experimentation indicates that the PL of the hydrothermally synthesized as-prepared CDs mainly arises from the CDs' molecular state, rather than from the quantum size effect (Fig. 7). The surface chemical groups on the CDs (corresponding to their molecular state, probably the imide groups) are dominant in determining the optical properties of the CDs, which explains the blue PL emissions of most hydrothermally carbonized CDs and the brighter emissions of those prepared under milder conditions [10]. At the same time, the CDs' highly carbonized cores are poorly crystallized, mainly exhibiting light-absorbing properties. In the initial stage of the carbonization process, polymer-like species (such as those found in f1) with abundant surface chemical groups and no carbonized cores are obtained; these exhibit strong fluorescence (high QY). As the carbonization proceeds, freshly carbonized species exist on the surface of CDs with abundant chemical groups. These show similarly strong fluorescence, but the highly carbonized cores have relatively weak fluorescence and absorb the outer components' emitted fluorescence, causing a QY

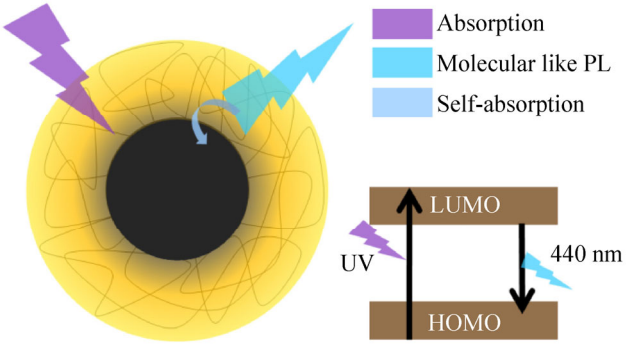

Figure 7 Scheme of the proposed PL mechanism of the CDs.

decrease. For the highly carbonized CDs, the amount of surface chemical groups significantly decreases and the carbonized cores become the majority of the particles. This induces a heavy loss of fluorescence from the outer components, and yields the lowest QY among the CDs in all fractions. Thus, the hydrophilicity gradient separation method provided an effective way to separate non-sedimental species such as CDs. Based on the separation experiments, new advances were made toward the comprehensive understanding of the optical properties and rational synthetic design of CDs.

4 Conclusions

A hydrophilicity gradient ultracentrifuge separation method was established to separate CDs synthesized from citric acid and ethylenediamine. Clusters of CDs were used as the starting state, and the hydrophilicity differences among the CDs were used to realize their separation in a gradient consisting of four water/ethanol ratio layers. The clustered CDs were successfully de-clustered and separated, essentially according to their differences in degree of carbonization, in the subsequent centrifugation. The proposed technique offers a general, novel, and effective strategy for the separation of non-sedimental species. This work provides important evidence for understanding the PL mechanism of CDs. After careful analysis of the CDs in typical fractions regarding their morphology, size, crystallinity, composition, QY, and transient PL, we concluded that the PL behaviors of the as-prepared hydrothermally carbonized CDs mainly arose from the radiative recombination of excitons related to the CDs' surface chemical groups, as opposed to the difference in size of the CDs' carbonized cores.

Acknowledgements

This work was supported by the National Natural Science Foundation of China (Nos. 21101012, 21125101 and 21271018), the Fundamental Research Funds for the Central Universities (No. YS1406), the National Basic Research Program of China (No. 2011CBA00503), Program for Changjiang Scholars and Innovative Research Team in University.

Electronic Supplementary Material: Supplementary material (additional HRTEM images, separation method studies, size distribution of separated fractions and spectroscopic studies) is available in the online version of this article at http://dx.doi.org/10.1007/s12274-015-0786-y.

References

[1] Xu, X. Y.; Ray, R.; Gu, Y. L.; Ploehn, H. J.; Gearheart, L.; Raker, K.; Scrivens, W. A. Electrophoretic analysis and purification of fluorescent single-walled carbon nanotube fragments. *J. Am. Chem. Soc.* **2004**, *126*, 12736–12737.

[2] Baker, S. N.; Baker, G. A. Luminescent carbon nanodots: Emergent nanolights. *Angew. Chem., Int. Ed.* **2010**, *49*, 6726–6744.

[3] Li, H. T.; Kang, Z. H.; Liu, Y.; Lee, S. T. Carbon nanodots: Synthesis, properties and applications. *J. Mater. Chem.* **2012**, *22*, 24230–24253.

[4] Ding, C. Q.; Zhu, A. W.; Tian, Y. Functional surface engineering of C-dots for fluorescent biosensing and *in vivo* bioimaging. *Acc. Chem. Res.* **2014**, *47*, 20–30.

[5] Cao, L.; Wang, X.; Meziani, M. J.; Lu, F. S.; Wang, H. F.; Luo, P. G.; Lin, Y.; Harruff, B. A.; Veca, L. M.; Murray, D. et al. Carbon dots for multiphoton bioimaging. *J. Am. Chem. Soc.* **2007**, *129*, 11318–11319.

[6] Ray, S. C.; Saha, A.; Jana, N. R.; Sarkar, R. Fluorescent carbon nanoparticles: Synthesis, characterization, and bioimaging application. *J. Phys. Chem. C* **2009**, *113*, 18546–18551.

[7] Li, H. T.; He, X. D.; Kang, Z. H.; Huang, H.; Liu, Y.; Liu, J. L.; Lian, S. Y.; Tsang, C. H. A.; Yang, X. B.; Lee, S. T. Water-soluble fluorescent carbon quantum dots and photocatalyst design. *Angew. Chem., Int. Ed.* **2010**, *49*, 4430–4434.

[8] Shi, W. B.; Wang, Q. L.; Long, Y. J.; Cheng, Z. L.; Chen, S. H.; Zheng, H. Z.; Huang, Y. M. Carbon nanodots as peroxidase mimetics and their applications to glucose detection. *Chem. Commun.* **2011**, *47*, 6695–6697.

[9] Choi, H.; Ko, S. J.; Choi, Y.; Joo, P.; Kim, T.; Lee, B. R.; Jung, J. W.; Choi, H. J.; Cha, M.; Jeong, J. R. et al. Versatile surface plasmon resonance of carbon-dot-supported silver nanoparticles in polymer optoelectronic devices. *Nat. Photonics* **2013**, *7*, 732–738.

[10] Zhu, S. J.; Meng, Q. N.; Wang, L.; Zhang, J. H.; Song, Y. B.; Jin, H.; Zhang, K.; Sun, H. B.; Wang, H. Y.; Yang, B. Highly photoluminescent carbon dots for multicolor patterning, sensors, and bioimaging. *Angew. Chem., Int. Ed.* **2013**, *52*, 3953–3957.

[11] Sun, Y. P.; Zhou, B.; Lin, Y.; Wang, W.; Fernando, K. A. S.; Pathak, P.; Meziani, M. J.; Harruff, B. A.; Wang, X.; Wang, H. F. et al. Quantum-sized carbon dots for bright and colorful photoluminescence. *J. Am. Chem. Soc.* **2006**, *128*, 7756–7757.

[12] Jiang, H. Q.; Chen, F.; Lagally, M. G.; Denes, F. S. New strategy for synthesis and functionalization of carbon nanoparticles. *Langmuir* **2010**, *26*, 1991–1995.

[13] Liu, H. P.; Ye, T.; Mao, C. D. Fluorescent carbon nanoparticles derived from candle soot. *Angew. Chem., Int. Ed.* **2007**, *46*, 6473–6475.

[14] Bourlinos, A. B.; Stassinopoulos, A.; Anglos, D.; Zboril, R.; Georgakilas, V.; Giannelis, E. P. Photoluminescent carbogenic dots. *Chem. Mater.* **2008**, *20*, 4539–4541.

[15] Peng, J.; Gao, W.; Gupta, B. K.; Liu, Z.; Romero-Aburto, R.; Ge, L. H.; Song, L.; Alemany, L. B.; Zhan, X. B.; Gao, G. H. et al. Graphene quantum dots derived from carbon fibers. *Nano Lett.* **2012**, *12*, 844–849.

[16] Lingam, K.; Podila, R.; Qian, H. J.; Serkiz, S.; Rao, A. M. Evidence for edge-state photoluminescence in graphene quantum dots. *Adv. Funct. Mater.* **2013**, *23*, 5062–5065.

[17] Wang, L.; Zhu, S. J.; Wang, H. Y.; Qu, S. N.; Zhang, Y. L.; Zhang, J. H.; Chen, Q. D.; Xu, H. L.; Han, W.; Yang, B. et al. Common origin of green luminescence in carbon nanodots and graphene quantum dots. *ACS Nano* **2014**, *8*, 2541–2547.

[18] Liu, R. L.; Wu, D. Q.; Liu, S. H.; Koynov, K.; Knoll, W.; Li, Q. An aqueous route to multicolor photoluminescent carbon dots using silica spheres as carriers. *Angew. Chem., Int. Ed.* **2009**, *48*, 4598–4601.

[19] Arnold, M. S.; Green, A. A.; Hulvat, J. F.; Stupp, S. I.; Hersam, M. C. Sorting carbon nanotubes by electronic structure using density differentiation. *Nat. Nanotechnol.* **2006**, *1*, 60–65.

[20] Bai, L.; Ma, X. J.; Liu, J. F.; Sun, X. M.; Zhao, D. Y.; Evans, D. G. Rapid separation and purification of nanoparticles in organic density gradients. *J. Am. Chem. Soc.* **2010**, *132*, 2333–2337.

[21] Mastronardi, M. L.; Hennrich, F.; Henderson, E. J.; Maier-Flaig, F.; Blum, C.; Reichenbach, J.; Lemmer, U.; Kübel, C.; Wang, D.; Kappes, M. M. et al. Preparation of monodisperse silicon nanocrystals using density gradient ultracentrifugation. *J. Am. Chem. Soc.* **2011**, *133*, 11928–11931.

[22] Ma, X. J.; Kuang, Y.; Bai, L.; Chang, Z.; Wang, F.; Sun, X. M.; Evans, D. G. Experimental and mathematical modeling studies of the separation of zinc blende and wurtzite phases of CdS nanorods by density gradient ultracentrifugation. *ACS Nano* **2011**, *5*, 3242–3249.

[23] Zhang, C. L.; Luo, L.; Luo, J.; Evans, D. G.; Sun, X. M. A process-analysis microsystem based on density gradient centrifugation and its application in the study of the galvanic replacement mechanism of Ag nanoplates with $HAuCl_4$. *Chem. Commun.* **2012**, *48*, 7241–7243.

[24] Song, S.; Kuang, Y.; Liu, J. F.; Yang, Q.; Luo, L.; Sun, X. M. Separation and phase transition investigation of Yb^{3+}/Er^{3+} co-doped $NaYF_4$ nanoparticles. *Dalton Trans.* **2013**, *42*, 13315–13318.

[25] Horn, D.; Rieger, J. Organic nanoparticles in the aqueous phase—theory, experiment, and use. *Angew. Chem., Int. Ed.* **2001**, *40*, 4330–4361.

[26] Aubry, J.; Ganachaud, F.; Addad, J. P. C.; Cabane, B. Nanoprecipitation of polymethylmethacrylate by solvent shifting: 1. Boundaries. *Langmuir* **2009**, *25*, 1970–1979.

[27] Zheng, M.; Xie, Z. G.; Qu, D.; Li, D.; Du, P.; Jing, X. B.; Sun, Z. C. On-off-on fluorescent carbon dot nanosensor for recognition of chromium(VI) and ascorbic acid based on the inner filter effect. *ACS Appl. Mater. Inter.* **2013**, *5*, 13242–13247.

[28] Song, Y. B.; Zhu, S. J.; Xiang, S. Y.; Zhao, X. H.; Zhang, J. H.; Zhang, H.; Fu, Y.; Yang, B. Investigation into the fluorescence quenching behaviors and applications of carbon dots. *Nanoscale* **2014**, *6*, 4676–4682.

[29] Tang, L. B.; Ji, R. B.; Li, X. M.; Bai, G. X.; Liu, C. P.; Hao, J. H.; Lin, J. Y.; Jiang, H. X.; Teng, K. S.; Yang, Z. B. et al. Deep ultraviolet to near-infrared emission and photoresponse in layered N-doped graphene quantum dots. *ACS Nano* **2014**, *8*, 6312–6320.

[30] Wei, W. L.; Xu, C.; Wu, L.; Wang, J. S.; Ren, J. S.; Qu, X. G. Non-enzymatic-browning-reaction: A versatile route for production of nitrogen-doped carbon dots with tunable multicolor luminescent display. *Sci. Rep.* **2014**, *4*, 3564.

[31] Li, W.; Zhang, Z. H.; Kong, B.; Feng, S. S.; Wang, J. X.; Wang, L. Z.; Yang, J. P.; Zhang, F.; Wu, P. Y.; Zhao, D. Y. Simple and green synthesis of nitrogen-doped photoluminescent carbonaceous nanospheres for bioimaging. *Angew. Chem., Int. Ed.* **2013**, *52*, 8151–8155.

[32] Wang, X. Y.; Qu, L. H.; Zhang, J. Y.; Peng, X. G.; Xiao, M. Surface-related emission in highly luminescent CdSe quantum dots. *Nano Lett.* **2003**, *3*, 1103–1106.

[33] Zhao, K.; Li, J.; Wang, H. Z.; Zhuang, J. Q.; Yang, W. S. Stoichiometric ratio dependent photoluminescence quantum yields of the thiol capping CdTe nanocrystals. *J. Phys. Chem. C* **2007**, *111*, 5618–5621.

[34] Huang, L. W.; Liao, Q.; Shi, Q.; Fu, H. B.; Ma, J. S.; Yao, J. N. Rubrene micro-crystals from solution routes: Their crystallography, morphology and optical properties. *J. Mater. Chem.* **2010**, *20*, 159–166.